PCCP

Centerband-Only-Detection-of-Exchange
^{31}P nuclear magnetic resonance and phospholipid lateral diffusion: Theory, simulation and experiment

Angel Lai, Qasim Saleem and Peter M. Macdonald[a]

Department of Chemistry

University of Toronto

and

Department of Chemical and Physical Sciences

University of Toronto Mississauga

3359 Mississauga Road North

Mississauga, Ontario, Canada L5L 1C6

[a] Email: pm.macdonald@utoronto.ca

Centerband-only-detection-of-exchange (CODEX) ^{31}P NMR lateral diffusion measurements were performed on dimyristoylphosphatidylcholine (DMPC) assembled into large unilamellar spherical vesicles. Optimization of sample and NMR acquisition conditions provided significant sensitivity enhancements relative to an earlier first report (Q. Saleem, A. Lai, H. Morales, and P.M. Macdonald, *Chem. Phys. Lipids*, 2012, **165**, 721.) An analytical description was developed that permitted the extraction of lateral diffusion coefficients from CODEX data, based on a Gaussian-Diffusion-on-a-Sphere model (A. Ghosh, J. Samuel, and S. Sinha, S., *Europhys. Lett.*, 2012, **98**, 30003-p1.) as relevant to CODEX ^{31}P NMR measurements on a population of spherical unilamellar phospholipid bilayer vesicles displaying a distribution of vesicle radii.

1 Introduction

Lateral diffusion of lipids and proteins is essential to the function of biological membranes.[1] The vast majority of lateral diffusion measurements have been made using high-sensitivity fluorescence-based techniques such as fluorescence recovery after photobleaching (FRAP),[2] fluorescence correlation spectroscopy (FCS)[3] and, more recently, single particle tracking (SPT).[4] NMR-based diffusion measurements, whether employing Pulsed Field Gradient (PFG) or Exchange Spectroscopy (EXSY) methods, have enjoyed far less popularity in lateral diffusion studies due to sensitivity and resolution issues. However, the combination of magic angle spinning (MAS) with PFG[5] or EXSY[6] NMR ameliorates both the sensitivity and resolution limitations associated with the broad resonances inherent to biological membranes. As an example, we recently reported the first use of the Centerband-Only-Detection-of-Exchange (CODEX) technique, originated by Schmidt-Rohr and coworkers,[6] to measure lateral diffusion of phospholipids via ^{31}P NMR.[7]

In CODEX, orientation-dependent terms such as the chemical shift anisotropy (and others) are eliminated using fast MAS, with correspondingly increased sensitivity and enhanced resolution of different chemical species. The experiment is rendered sensitive to lateral diffusion by reintroducing (recoupling) the orientation dependence using radio-frequency (*rf*) pulses carefully synchronised with respect to the period of the spinning rotor. During a subsequent "exchange" period, any lateral diffusion of a phospholipid around the radius of curvature of a spherical lipid bilayer vesicle alters its orientation with respect to the magnetic field. The new orientation is then monitored via a second recoupling period and any difference in orientation relative to the original produces a loss of signal proportional to the extent of lateral diffusion.

In our earlier "proof-of-principle" article, the focus was on demonstrating the feasibility of CODEX ^{31}P NMR for measuring lateral diffusion of phospholipids in bilayer membranes.[7] Those first experiments employed small bilayer vesicles, while the CODEX diffusive decays were fit with a phenomenological equation that accounted for the combined contributions of lateral diffusion and whole vesicle tumbling on phospholipid reorientations. Here we present what we regard as a "gold standard" CODEX ^{31}P NMR lateral diffusion measurement on dimyristoylphosphatidylcholine (DMPC) assembled into large unilamellar spherical vesicles. Consequently, the contribution of vesicle tumbling is negligible, and there is a profound improvement in sensitivity, abetted by optimization of experimental conditions. In addition, we present an analytical description that permits the extraction of a lateral diffusion coefficient from the observed intensity decay in CODEX experiments, based on the Gaussian-Diffusion-on-a-Sphere model equations of Ghosh et al[8] and the powder average CODEX intensity equations of deAzevedo et al[9] as relevant to ^{31}P NMR measurements on a population of spherical unilamellar phospholipid bilayer vesicles displaying a distribution of vesicle radii.

2　Lateral diffusion coefficients and CODEX decays

2.1　Fundamentals of CODEX ^{31}P NMR

Fig. 1 illustrates the CODEX ^{31}P NMR pulse sequence used here for measuring phospholipid lateral diffusion in spherical lipid bilayer vesicles, where a single 90° direct excitation pulse replaces the more conventional cross polarization excitation. Proton {^{1}H} dipolar decoupling is applied during the recoupling periods and during signal acquisition. The sample is undergoing fast MAS, i.e., the spinning speed ν_r is greater than the size of the ^{31}P chemical shift anisotropy

(CSA) δ. All *rf* pulse timings are synchronized with the MAS rotor period, $t_r = 1/v_r$. Under fast MAS the orientation-dependent anisotropic chemical shift terms are eliminated, so only the orientation-independent isotropic chemical shift terms remain. While this maximizes resolution of different chemically shifted phospholipid species, the orientation-dependent terms upon which lateral diffusion measurements rely are lost. In CODEX, the ^{31}P CSA is recoupled during the initial and final recoupling periods through 180° pulses placed at half rotor periods ($t_r/2$). The 180° pulses produce a net accumulation of phase Φ_i in the xy plane over one recoupling period, depending on the details of the orientation of the CSA tensor relative to the spinning axis (see below). For the case of phospholipids within a spherical bilayer vesicle, if lateral diffusion around the spherical vesicle's radius of curvature occurs during the mixing time ($t_m = Nt_r$), then the phase Φ_1 acquired during the initial recoupling period will differ from the phase Φ_2 acquired during the final recoupling period, and signal cancellation will occur. In general, increasing the number of 180° pulses ($M = 1,3,5\ldots, where\ M = 2m + 1$), increases the sensitivity of CODEX to the motion being detected;[6,9] however, the duration of the recoupling periods is limited by the correlation time of that motion and the spin-spin relaxation time (T_2). From the decay of the CODEX signal intensity, $S(t_m, \delta M t_r)$, with increasing mixing time, one may extract the lateral diffusion coefficient. For each mixing time, an accompanying reference signal $S_0(t_m, \delta M t_r)$ is measured, wherein t_m and the final z-filter (t_z) have been interchanged in order that any attenuation due to longitudinal relaxation during t_m can be factored out.

Figure 1

2.2 Rotational correlation times and CODEX decays

In our earlier report,[7] the CODEX mixing time intensity dependence was expressed in terms of an exponential decay with a time constant corresponding to the rotational correlation time for a spherical bilayer vesicle of radius R_i.

$$\frac{S(t_m, \delta M t_r, R_i)}{S_0(t_m, \delta M t_r, R_i)} = \exp\left(-\frac{t_m}{\tau_c(R_i, D_{rot})}\right) \tag{1}$$

The rotational correlation time $\tau_c(R_i, D_{rot})$ follows from Bloembergen et al[10] and Abragam[11] who described rotational effects on dipolar NMR relaxation by invoking the Debye model for rotational diffusion with a rotational diffusion coefficient D_{rot} given by the Stokes formula.

$$D_{rot} = \frac{k_B T}{8\pi\eta R_i} \tag{2}$$

Since the correlation functions for dipolar NMR relaxation depend on spherical harmonic functions of order $l=2$, the rotational correlation time is related to the diffusion constant for rotation as follows

$$\frac{1}{\tau_c(R_i, D_{rot})} = \frac{D_{rot}}{R_i^2} l(l+1) = \frac{6 D_{rot}}{R_i^2} \tag{3}$$

For the case of a spherical lipid bilayer vesicle, Bloom et al.[12] assumed independent contributions to D_{rot} from overall vesicle rotational tumbling (D_{tum}) and lateral diffusion of individual lipids around the radius of curvature of the spherical vesicle (D_{lat})

$$D_{rot} = D_{tum} + D_{lat} \tag{4}$$

Assuming that overall vesicle tumbling obeys the Stokes formula, one obtains

$$\frac{1}{\tau_c(R_i, D_{rot})} = \frac{6}{R_i^2}\left(\frac{k_B T}{8\pi\eta R_i} + D_{lat}\right) = \frac{3 k_B T}{4\pi\eta R_i^3} + \frac{6 D_{lat}}{R_i^2} \tag{5}$$

For a distribution of vesicle sizes, the CODEX decay is a weighted sum of terms as per Eq. (1). The probability density of vesicle radii can be determined using, for example, dynamic light

scattering. Given knowledge of the viscosity and the vesicle size distribution, the lateral diffusion coefficient becomes the sole fitting parameter for analyzing CODEX diffusive decays. This approach is straightforward to implement and provides lateral diffusion coefficients in general agreement with literature values.[7] However, the observed CODEX decays are influenced by the combined effects of the chemical shift anisotropy and the duration of the recoupling period, as well as the lateral diffusion coefficient and the vesicle radius. In order to incorporate such considerations into the process of extracting the lateral diffusion coefficient, a more detailed approach is required, as follows.

2.3   Powder average diffusion probabilities and CODEX decays

A more rigorous approach for extracting lateral diffusion coefficients from CODEX decays is to calculate the complete powder average CODEX signal, commencing with the normalized CODEX signal intensity as given by deAzevedo et al,[9]

$$\frac{S(t_m, \delta M t_r)}{S_0(t_m, \delta M t_r)} = \langle cos(|\Phi_2| - |\Phi_1|)\rangle \tag{6}$$

where Φ_i is the phase angle acquired during a given CODEX recoupling period containing M 180° pulses, while the angled brackets represent the powder average over all spins. The phase acquired during a given CODEX recoupling period is,

$$|\Phi_i| = \left| M \int_0^{t_r/2} \omega_i(t)dt \right| \tag{7}$$

where the precession frequency $\omega_i(t)$ becomes time-dependent due to magic angle spinning. For the case of an axially symmetric chemical shielding tensor, as relevant to the residual ^{31}P chemical shielding tensor of a phospholipid within a liquid-crystalline bilayer, the time-

dependent precession frequency due to rotation at an angular frequency (ω_r) was derived by Munowitz and Griffin.[13]

$$\omega_i(t) = \frac{\delta}{2}\left[sin^2\beta_i\,cos2(\alpha_i + \omega_r t) - \sqrt{2}sin2\beta_i\,cos(\alpha_i + \omega_r t)\right] \tag{8}$$

The angles β_i and α_i are the polar and azimuthal angles, respectively, defining the orientation of the unique axis σ_z within the reference frame attached to the spinning axis as shown in Fig. 2, with $\alpha = 0$ arbitrarily in the plane defined by the magnetic field and the spinning axis. For the CODEX case, where $t = t_r/2$, the accumulated phase during any dephasing / rephasing period is then

$$\Phi_i(M, t_r/2) = M\frac{\delta}{\omega_r}\sqrt{2}\sin 2\beta_i \sin \alpha_i \tag{9}$$

where it is assumed that the recoupling periods are short relative to the correlation time for motion. Thus, the quantity $cos(|\Phi_2| - |\Phi_1|)$ can be calculated for any combination of initial orientation defined by the set of angles $\{\beta_1, \alpha_1\}$ and final orientation defined by the set of angles $\{\beta_2, \alpha_2\}$.

Figure 2

The final orientation $\{\beta_2, \alpha_2\}$ is the result of a diffusive jump through some angle θ commencing from the initial orientation $\{\beta_1, \alpha_1\}$, as illustrated in Fig. 2. Due to the spherical symmetry, diffusive jumps in any direction relative to the initial orientation are equally probable, yet each direction produces a different final orientation. Thus, it is necessary to specify both the diffusive jump distance and direction, corresponding to the polar and azimuthal angles θ and ϕ, respectively, as defined in the coordinate system fixed on the original orientation, per the geometry detailed in Fig. 2. Using Euler angles and rotation matrices, following the convention of Rose,[14] one may obtain the trigonometric term in Eq. (9) for the final orientation $\{\beta_2, \alpha_2\}$ in

terms of the initial orientation $\{\beta_1, \alpha_1\}$ plus the set of angles defining jump distance and direction $\{\theta, \phi\}$ as per Eq. (10).

$$
\begin{aligned}
\sin 2\beta_2 \sin \alpha_2 \\
= \sin 2\beta_1 \sin \alpha_1 \left[1 - \sin^2 \theta \left(1 + \cos^2 \phi\right)\right] \\
- \sin \beta_1 \cos \alpha_1 \; \sin^2 \theta \sin 2\phi \\
+ \left(\cos 2\beta_1 \sin \alpha_1 \cos \phi + \; \cos \beta_1 \cos \alpha_1 \sin \phi\right) \sin 2\theta
\end{aligned}
\tag{10}
$$

Thus, the quantity $\cos(|\Phi_2| - |\Phi_1|)$ can be obtained for any set of angles $\{\beta_1, \alpha_1, \theta, \phi\}$. Since all azimuthal jump angles $0 < \phi < 360$ are equally probable, it is convenient to calculate the average $\langle\cos(|\Phi_2| - |\Phi_1|)\rangle_\phi$ for any set of angles $\{\beta_1, \alpha_1, \theta\}$. Likewise, all azimuthal angles $0 < \alpha_1 < 360$ being equally probable, it is convenient to then calculate the average $\langle\langle\cos(|\Phi_2| - |\Phi_1|)\rangle_\phi\rangle_{\alpha_1}$ for any set of angles $\{\beta_1, \theta\}$. The resulting matrix of this average phase difference for all $0 \leq \beta_1 \leq 180$ and $0 \leq \theta \leq 180$ is shown in Fig. 4A for the case $M = 3, \frac{3}{2}\delta = 45 \; ppm$ and $v_r = 6500$ Hz. It is evident that the CODEX diffusive decay will be most sensitive to diffusive jump angles in the approximate range $0 < \theta < 45$, in accord with the conclusions of deAzevedo et al.[9]

For diffusion on a sphere, the probability distribution as a function of time is obtained as a solution to the rotational version of Fick's law of diffusion. The formal solution is written as an expansion in spherical harmonics, where for a given initial distribution $P(\theta,0)$ at time zero, the final distribution in θ at time τ is

$$
P(\theta, \tau) = \frac{sin\theta}{2} \sum_{l=0}^{\infty} (2l + 1) P_l(cos\theta) e^{-l(l+1)\tau/2}
\tag{11}
$$

where $P_l(cos\theta)$ is a Legendre polynomial of order l and τ is a dimensionless time variable. Such an approach can be used, for example, to analyze static two-dimensional exchange ^{2}H NMR

spectra of deuterated phospholipid bilayers on spherical solid supports in order to extract lateral

diffusion coefficients.[15] From a practical perspective, the fact of dealing with an infinite series

makes simulation unwieldy. Moreover, care must be exercised if truncating the series, since

spurious oscillations may result.

A closed form expression closely approximating the probability distributions obtained

with the infinite series of spherical harmonics solution has been derived by Ghosh et al,[8] which

the authors term a "Gaussian" for diffusion on the sphere,

$$P(\theta,\tau) = \frac{N(\tau)}{\tau}\sqrt{\theta\,sin\theta}\;e^{-\frac{\theta^2}{2\tau}} \tag{12}$$

where the normalization constant $N(\tau)$ is defined such that

$$\int_0^\pi d\theta\,P(\theta,\tau) = 1 \tag{13}$$

while the dimensionless time variable τ is,

$$\tau = \frac{2D_{lat}t_m}{R^2} \tag{14}$$

with D_{lat} being the lateral diffusion coefficient and R the radius of the sphere. Fig. 3 illustrates

how $P(\theta,\tau)$ varies with θ according to Eq. (12), for several different mixing times given values of

the parameters $D_{lat} = 1.0$ x 10^{-12} m²s⁻¹ and $R = 350$ x 10^{-9} m of relevance here.

Figure 3

Each set of angles $\{\beta_1,\,\theta\}$ will have a corresponding weighting factor $P(\beta_1)P(\theta,\tau)$,

where $P(\beta_1) = sin\beta_1$ is the geometric weighting factor while $P(\theta,\tau)$ is obtained from Eq. (11).

The resulting matrix of normalized weighting factors $P(\beta_1)P(\theta,\tau)$ for all $0 \leq \beta_1 \leq 180$ and

$0 \leq \theta \leq 180$ is shown in Fig. 4B for the case $D_{lat} = 1.0$ x 10^{-12} m²s⁻¹, $R = 350$ x 10^{-9} m and $t_m = 10t_r$. Fig. 4C shows the weighted CODEX intensity, i.e., $P(\beta_1)P(\theta,\tau)\langle\langle cos(|\Phi_2| - |\Phi_1|)\rangle_\phi\rangle_{\alpha_1}$,

for all $\{\beta_1, \theta\}$. The powder average CODEX intensity is then simply the sum of such quantities over all $\{\beta_1, \theta\}$.

Figure 4

In order to fit CODEX decays and extract lateral diffusion coefficients, it is convenient, from a practical perspective, to first calculate $\langle\langle\cos(|\Phi_2| - |\Phi_1|)\rangle_\phi\rangle_{\alpha_1}$ for all $\{\beta_1, \theta\}$ since values of M, δ and ω_r are generally constant for a given set of measurements. The normalized weighting factors $P(\beta_1)P(\theta, \tau)$ are then calculated for particular known values of R and t_m, and an assumed value of D_{lat}. The powder average CODEX intensity is calculated as above, and this is repeated for each different vesicle radius in the sample for any one mixing time. The CODEX intensity at that mixing time for an assumed lateral diffusion coefficient is the weighted average according to the number density $P(R_i)$ of lipids in vesicles of radius R_i in the sample. The process is then repeated for each mixing time. The resulting simulated CODEX diffusive decay curve is fitted to the experimental data in order to obtain the best estimate of the lateral diffusion coefficient. On a desktop personal computer, such fittings require only a minute or two to complete.

2.4   Simulated powder-average CODEX decays and Gaussian-Diffusion-on-a-Sphere

Fig.5 shows simulations of the powder-average CODEX mixing time-dependent decays predicted using the Gaussian-Diffusion-on-a-Sphere model as a function of the four principle variables encountered in CODEX lateral diffusion measurements: the number of recoupling pulses M, the CSA, the vesicle radius R and the lateral diffusion coefficient D_{lat}. In these simulations relaxation effects during the recoupling or mixing periods have been ignored and only lateral diffusion during the mixing time has been taken into account.

10

Fig. 5A shows the profound increase in sensitivity to lateral diffusion with increasing *M,* here for the particular case $\frac{3}{2}\delta = 45\ ppm$, *R*=350 nm and $D_{lat} = 1 \times 10^{-11}\ m^2 s^{-1}$. This is an aspect of the CODEX experiment not reflected by the straightforward rotational correlation time dependency contained in Eq. (1). For the case *M*=1, the decay ceases at roughly *S/S₀*=0.63, and is insensitive to further increases in the mixing time beyond roughly *N*=25. Moreover, any dependence of the intensity decay on the lateral diffusion coefficient and/or the vesicle radius is likewise compressed into this relatively narrow range. The relative insensitivity with *M*=1 is simply a reflection of the quantity *Mδ* appearing in Eq. 9, which scales the phase difference $cos(|\Phi_2| - |\Phi_1|)$. While *M* is under experimental control, the value of *δ,* being sample dependent, is not. For the case *M*=5, the signal intensity falls rapidly towards zero within a relatively short number of rotor periods, leaving relatively few intensity data points accessible at the particular spinning speed $\nu_r = 6500\ Hz$ available with our MAS probe, thus compromising the reliability of any fits to experimental data. The middle case, *M*=3, is thus the optimal choice. In particular, one observes that at long mixing times the signal intensity approaches zero, in accord with the prediction that $S_\infty/S_0 \rightarrow f_m/W$, where S_∞/S_0 is the CODEX signal at long mixing times, i.e., $t_m >> t_c, f_m$ is the fraction of mobile species and *W* is the number of sites.[6,9] Thus, for fluid lipids in large bilayer vesicles, one expects $f_m \rightarrow 1$, while $W \rightarrow \infty$, so that $S_\infty/S_0 \rightarrow 0$. Consequently, further simulations below (and experiments to follow) will focus on the case *M*=3.

Fig. 5B illustrates the predicted influence of the CSA for the case *M*=3, *R*=350 nm and $D_{lat} = 1 \times 10^{-11}\ m^2 s^{-1}$. As expected, larger values of the CSA produce greater sensitivity to lateral diffusion as per Eq. 9. The case $\frac{3}{2}\delta = 45\ ppm$ is most relevant to DMPC in the liquid-crystalline state, while $\frac{3}{2}\delta = 60\ ppm$ is relevant to gel state DMPC. A smaller residual CSA can

result from additional motional averaging such as vesicle tumbling or high curvature. Different phospholipid species can exhibit somewhat different values of the CSA. Thus, if mixtures of phospholipids were being investigated it would be important to know the CSA of each.

Fig. 5C illustrates the predicted influence of the vesicle radius for the case $\frac{3}{2}\delta = 45\ ppm$, M=3 and D_{lat} = 1 x 10^{-11} m^{2}s^{-1}. Clearly, the distribution of vesicle radii in the sample needs to be taken into account when simulating experimental CODEX decays. In particular, the decay curve at short mixing times will be dominated by the behavior of the smaller radii vesicles, and at longer mixing times by that of the larger radii vesicles.

In Fig. 5D, the sensitivity to the lateral diffusion coefficient is simulated for the specific case of $\frac{3}{2}\delta = 45\ ppm$, M=3 and R=350 nm, the latter being representative of a typical vesicle radius in our experiments. Lateral diffusion coefficients ranging over several orders of magnitude, spanning the range of values expected experimentally, may be differentiated. For very slow diffusion coefficients, much longer mixing times eventually produce signal intensities approaching zero, but such instances are limited in practical terms by T$_1$ relaxation which has been ignored in these simulations. However, when a very fast lateral diffusion coefficient was simulated, e.g., D_{lat} = 1 x 10^{-10} m^{2}s^{-1}, anomalous oscillations appeared at even relatively short mixing times. These became apparent whenever a particular combination of diffusion coefficient, vesicle radius and mixing time produced a predicted jump angle in the Gaussian-Diffusion-on-a-Sphere equation that significantly exceeded one radian, i.e., the limit in which this equation was intended to function.

A further consequential conclusion to be drawn from such simulations is that for the typical vesicle radius and lateral diffusion coefficient values expected to be encountered experimentally, there will be a significant loss of intensity for the shortest experimentally-

accessible mixing time, $t_m = t_r$, due to lateral diffusion alone. And this intensity loss will increase with increasing number of recoupling pulses, or faster lateral diffusion, or smaller vesicle radius. For example, in the typical case of R=350 nm and D_{lat} = 1 x 10^{-11} m^{2}s^{-1} shown in Fig. 5A, with increasing number of recoupling pulses the intensity at time point $t_m = t_r$ decreases from 0.97 for M=1, to 0.75 for M=3, and further to 0.49 for M=5. To properly extract lateral diffusion coefficients via simulations of experimental CODEX decay curves, it will be imperative to take such effects into account.

Figure 5

3 Experimental methods

3.1 Materials

1,2-dimyristoyl-*sn*-glycero-3-phosphocholine (DMPC) and 1,2-dioleoyl-*sn*-glycero-3-phosphoethanolamine-N-(7-nitro-2-1,3-benzoxadiazol-4-yl (NBD-PE) were purchased from Avanti Polar Lipids (Alabaster, AL). 3-O (2-aminoethoxyethyloxyethyl)-carbamyl cholesterol (AECHO) was synthesized as described elsewhere.[16] All other reagents were purchased from Sigma-Aldrich (Oakville, ON, Canada).

3.2 Liposome preparation

Large unilamellar vesicles (LUV) were prepared by a dehydration/rehydration/extrusion method. DMPC was weighed out, and AECHO (5 mol%) and NBD-PE (0.5 mol%) were added to reach a total weight of 50 mg. The lipids were dissolved in a minimum volume of chloroform, which was then vortexed to ensure thorough mixing. The excess solvent was then dried off under a gentle stream of nitrogen and allowed to dry overnight in a vacuum dessicator to remove any remaining traces of solvent. MilliQ water was then heated to 35°C, and 2 mL was added to the dried lipid film to be hydrated for one hour while in a 35 °C water bath. The sample was then

subjected to five cycles of freeze-thaw-vortex, cycling between liquid nitrogen and a 60°C water bath. The resulting suspension of multilamellar vesicles (MLV) was then separated into two 1 mL batches, and each batch was extruded 25 times through a 0.1 μm polycarbonate membrane installed in a mini-extruder (Avanti Polar Lipids, Alabaster, AL) at 30°C. The resulting liposome suspensions were then combined and placed under vacuum overnight while in a 35°C water bath. A HEPES buffer (10 mM HEPES, 20 mM KCl, 1 mM EDTA, pH 7.4) was then heated to 35°C, and 2 mL was added to the dried lipid film, which was allowed to hydrate unperturbed for one hour in a 35°C water bath. The resulting suspension was then separated into two 1 mL batches, and each batch was extruded 25 times at 30°C through a 1.0 μm polycarbonate membrane installed in a mini-extruder. The liposome suspension was then concentrated and washed with buffer by four cycles of centrifugation at 14000 rpm for 30 minutes and re-suspension in HEPES buffer. The final centrifugation produced approximately 100 μL of LUV in the form of a pellet. A small sample of 2 μL of the DMPC LUV pellet was removed and diluted in 1 mL of HEPES buffer for dynamic light scattering and fluorescence measurements. The remaining LUV pellet was transferred to a 5 mm MAS rotor (sample volume approximately 120 μL) equipped with custom-built end-caps to prevent leakage.

3.3 Dynamic light scattering

A Malvern Zetasizer NanoZS (Malvern Instruments Ltd., Worcestershire, UK) was used to record the LUV mean size, size distribution and polydispersity (PDI). Approximately 1 mg of liposomes suspended in 1 mL HEPES buffer, filtered to remove dust and other exogenous particles, was placed in a glass cuvette with square aperture. All measurements were conducted at 25°C and performed in triplicate to ensure reproducibility. Scattering intensities at 633 nm were converted to LUV size using a DMPC refractive index of 1.348 obtained from the literature,[17] and the sample absorption measured via UV-Vis spectroscopy. The solvent

parameters for the HEPES buffer were generated using the NanoZS software, and size calibration beads were used to confirm accuracy.

3.4 Fluorescence-quenching lamellarity assay

A sodium dithionite fluorescence quenching assay was used to determine the number of lipid bilayers per liposome. Approximately 1 mg of liposomes containing 0.5 mol% NBD-PE were suspended in 2 mL HEPES buffer and placed in a glass cuvette with a square aperture. The sample was allowed to equilibrate at 15°C for 10 minutes prior to collecting measurements. The NBD-PE fluorescence was excited at 470 nm, and the resulting emission at 531 nm was monitored over time in a QuantaMaster PTI spectrofluorimeter (Photon Technology International, Lawrenceville, NJ). After an initial baseline was established, the measurement was paused, 20 μL of freshly-made 1 M sodium dithionite in 1 M Tris (pH 10) was added and mixed, and the measurement was resumed. After a new baseline was established, the measurement was paused again, 20 μL of 5% Triton (by weight) solution was added to disrupt completely the lipid bilayer integrity, and the measurement was again resumed.

3.5 NMR spectroscopy

^{31}P NMR spectra were acquired on a Varian INOVA 500 MHz NMR spectrometer using a VARIAN T3 triple-resonance MAS probe. The magic angle and field homogeneity of the spectrometer were optimized using KBr and adamantane respectively, prior to each experiment. Spectra for the liquid crystalline and gel phases were acquired at 35°C and 10°C respectively. Temperature was calibrated at a given spinning rate via the chemical shift of ^{79}Br in KBr.[18]

CODEX ^{31}P NMR spectra were acquired while spinning rotors at 6.5 kHz. TPPM proton decoupling,[19] with a ^{1}H B_1 field strength of 45 kHz, was applied during the recoupling and acquisition periods. Spectra were obtained in blocks of 32 scans per mixing time to ameliorate spectrometer drift. Pulse and receiver phases were cycled according to the modified phase table

appropriate to direct excitation as published by White and co-workers.[20] Typical acquisition parameters were as follows: a 90° pulse length of 6.2 µs, a recycle delay of 1.0 s, a dephasing/rephasing train of three 180° pulses, a spectral width of 25 kHz, and a 1 K data size. Typically, 512 transients were collected for each mixing time, and processed with an exponential multiplication equivalent to 30 Hz line broadening and zero-filled to 2 K prior to Fourier transformation.

4 Results and discussion

4.1 LUV Properties

CODEX ^{31}P NMR lateral diffusion measurements require knowledge of the distribution of vesicle radii across the DMPC/AECHO (95/5, mol/mol) LUV sample. 5 mol% AECHO was incorporated because it was found to enhance the ability to assemble larger unilamellar vesicles relative to 100% DMPC by virtue of the combination of cationic surface charge it imparts and the mechanical stability provided by its cholesteric ring. DLS results for the vesicle size and size distribution across a typical LUV sample are shown in Fig. 6. DLS results were little changed before and after having been subjected to CODEX measurements over the course of several hours. Thus, the effect of MAS at 6500 Hz was slight in that the LUV mean radius remained roughly constant at 400 nm, the size distribution remained mono-modal and the polydispersity was unchanged. Experiment times longer than roughly 48 hours were avoided as changes in LUV size and polydispersity became evident thereafter in DLS results.

Figure 6

DLS reports the number average vesicles of a given radius. However, CODEX will be sensitive to the population of lipids in a given population of vesicles of specified radius. This

will scale with the surface area of the vesicle, allowing the number average vesicle radius to be converted to a probability that the lipid population will occupy a vesicle of given radius, as shown in Fig. 6. The latter probabilities will be used for simulating CODEX decays.

As indicated by Eq. (5), the rate of rotational diffusion contains contributions from both lateral diffusion, scaling inversely as R^2, and overall vesicle rotational tumbling, scaling inversely as R^3. Thus, at a sufficiently large vesicle radius the contribution of overall vesicle tumbling becomes negligible. For a vesicle of radius 300 nm, at 35°C, assuming the viscosity of water, the rate of overall vesicle rotational tumbling is on the order of 40 s^{-1}. For the same size vesicle, assuming a typical lateral diffusion coefficient of 1x10^{-11} m^{2}s^{-1}, the rate of lateral diffusion is on the order of 666 s^{-1}. It is evident then that for the LUV employed here, one can expect the contribution of overall vesicle tumbling to the effective rate of rotational reorientation to be minimal, so that lateral diffusion effects will predominate.

The LUV used in our previous report[7] were roughly a factor of two smaller in radius than those shown in Fig. 6. Our intention at the time was to maximize the liposomal surface area in the MAS rotor in order to optimize the signal-to-noise ratio (SNR), given that smaller liposomes have a larger surface to volume ratio. However, it proved difficult to pack such smaller liposomes into the MAS rotor due to their relative buoyancy. The larger LUV employed in the present study pack readily under light centrifugation, resulting in an overall higher phospholipid density in the MAS rotor and correspondingly enhanced SNR.

For unilamellar vesicles, DLS dependably reports on the vesicle size distribution across the sample. For multilamellar vesicles, however, DLS reports only the size of the outermost bilayer. Thus, it is important to establish the lamellarity of the vesicles being examined. The results of a fluorescence quenching assay of vesicle lamellarity are shown in the Supplementary

17

Information (SI) Fig. S1, demonstrating that the vesicles were unilamellar and remained so over the experiment time.

DSC results showed that the gel-to-liquid-crystalline phase transition for the DMPC/AECHO (95/5, mol/mol) LUV occurred at 22°C, versus a temperature of 24°C for 100% DMPC. The cooperativity and enthalpy of the transition were nearly identical in the two cases. Thus the presence of 5 mol% AECHO had only nominal effects on the main gel-to-liquid-crystalline phase transition of DMPC.

4.2 CODEX ^{31}P NMR spectral optimization for phospholipids in LUV

Fig. 7 shows a series of CODEX ^{31}P NMR spectra acquired at $\nu_r = 6500\ Hz$ and M=3 as a function of increasing mixing time for LUV composed of 95/5 (mol/mol) DMPC/AECHO in 10 mM HEPES buffer, at a temperature of 35°C, i.e., above the main gel-to-liquid-crystalline phase transition temperature of 22°C. Corresponding spectra obtained at 10°C, i.e. in the gel phase, are provided in the SI, Fig. S2. In both cases a spinning speed of $\nu_r = 6500$ Hz sufficed to collapse the static spectra to an isotropic resonance with minimum spinning side band (SSB) intensity. (At 10°C only the n=±1SSB intensities remained significant.) Relative to the smaller LUV used previously,[7] the larger LUV used here yielded satisfactory SNR with far fewer scans, resulting in significantly shortened experiment times. This was largely due to better packing of the MAS rotor as described above.

Also shown in Fig, 7 are control experiments in which the mixing time (t_m) is held constant while the duration of the z-filter (t_z) is varied. Such measurements are intended to permit account to be taken of signal decay due to T_1 relaxation during the mixing time. As the figure shows, there is essentially no signal loss due to T_1 relaxation over the relevant time period. Given that the spin-lattice relaxation time T_1 for ^{31}P in liquid-crystalline phospholipid bilayers is

18

on the order ~ 700 ms, while the correlation time of motion for lateral diffusion is on the order <

10 ms, this result demonstrates that such referencing experiments are not essential for our

purposes. Importantly, this reduces by a factor of two the time required to perform phospholipid

lateral diffusion measurements via ^{31}P CODEX.

Additional optimizations of spectral acquisition conditions are described in the SI,

including the effects of pulse width errors (Fig. S3) and rotor synchronization errors (Fig. S4).

In particular, with the goal of achieving maximum SNR in a given experiment time, the recycle

delay for longitudinal relaxation was set shorter than the usual $5 \times T_1$. T_1 for the ^{31}P NMR signal

of these phospholipids being roughly 700 ms, an optimum recycle delay of 1 s was found to yield

the highest SNR for a set experiment time, as shown in Fig. S5. CODEX decays as a function of

increasing mixing time were essentially identical for recycle delays of 2 s and 10 s as shown in

Fig. S6. With LUV sample and NMR acquisition conditions optimized as above, a satisfactory

SNR could be obtained with our spectrometer / probe combination in as few as 512 scans for a

spectrum containing a single ^{31}P NMR resonance at a temperature above the gel-to-liquid-

crystalline phase transition. This means that an entire ^{31}P CODEX NMR lateral diffusion

measurement could be completed in roughly 1 hr, assuming a single lateral diffusion coefficient.

In cases of multiple resonances, or gel phase temperatures, or domains with different lateral

diffusion coefficients, experiment times would need to increase accordingly.

Figure 7

4.2 CODEX ^{31}P NMR intensity in LUV and the recoupling period

Eqs. (6)-(9) indicate that the strength of the CODEX recoupling and, hence, the sensitivity to the

motion under investigation, scales with the product $M\delta$. So, for smaller anisotropies δ, greater

recoupling may be achieved by increasing the number M of 180° pulses inserted during a given

recoupling period. However, relaxation processes during the recoupling periods, characterized

by an apparent time constant T_2^{rc}, produce signal loss proportional to $\exp(-\tau_{echo}/T_2^{rc})$, where the total echo time of the two recoupling periods is $\tau_{echo} = t_r(M+1)$, thus limiting the duration of the recoupling period that may be employed practically.

Fig. 8 compares the CODEX ^{31}P NMR normalized intensities obtained for MLV versus LUV as a function of increasing total echo time, at both 35°C and 10°C, for the shortest possible mixing time, $t_m = t_r = 154\ \mu s$. MLV were chosen as a basis for comparison because their large size (R >> 1 μm) means that the effective correlation time for rotational reorientation becomes very long. At 35°C the intensity decay with increasing M is far steeper with LUV than MLV. At 10°C, the intensity decay of MLV with increasing M is steeper than at 35°C, while that of LUV is shallower, such that the radical differences in the total echo time dependencies of MLV and LUV "master curves" at the higher temperature are significantly diminished at the lower temperature. The apparent T_2^{rc} extracted from the indicated exponential fittings are listed in Table 1. While the detailed values of the T_2^{rc} can vary from sample-to-sample, the trends evident in Fig. 8 are highly reproducible.

Table 1

Several studies have examined the origin of intensity losses during recoupling periods in CODEX experiments.[21,22] CODEX intensities in general will be a factor of two lower than experiments without recoupling since CODEX stores *cos* and *sin* components in separate transients. Intensity losses during recoupling may be factored into those originating with instrumental considerations and those due to intermediate time scale motions within the sample. Two common instrumental concerns in recoupling-type NMR experiments, assuming adequate rotor synchronization, are incomplete ^{1}H decoupling and the effects of finite π pulses.[22] Since cross polarization was not employed here, and the combination of MAS at 6500 Hz plus ^{1}H decoupling at a B_1 field strength of 45 kHz should effectively eliminate [31]P-^{1}H dipolar

interactions, at least at 35°C, other effects should be considered to explain the MLV versus LUV differences. Finite π pulse effects center on issues of finite excitation bandwidth, since we can ignore cross polarization effects in the present circumstances, while the finite length of the π pulse relative to the rotor period has only a small effect on the recoupling efficiency.[23] A conservative estimate of the excitation bandwidth of a π pulse of duration t_p is obtained from the width-at-half-height of the corresponding *sinc* function,[24] equal to ~$0.6/t_p$, which for a π pulse of duration 12.4 μs, as employed here, indicates an excitation bandwidth on the order of 48.4 kHz, i.e., ±24.2 kHz. This is certainly sufficient to excite the chemical shift range relevant here, i.e., δ = 30 – 40 ppm = 6 – 9 kHz. We conclude that in these instances such instrumental considerations are not the primary source of CODEX signal loss during the recoupling periods.

The intermediate time scale regime in the CODEX context refers to motions with correlation times in the vicinity of the recoupling period. CODEX was designed to examine slow motions with correlation times far longer than the recoupling time, limited only by the T_1. The presence of intermediate motions leads to irretrievable signal loss during the recoupling periods.[21,22] While signal loss itself is deleterious in that longer acquisition times are required, it has further consequences in that for heterogeneous samples, the recovered signal is biased towards longer correlation time components of the sample. Further, in the presence of intermediate motions the prediction $S_\infty/S_0 \rightarrow f_m/W$, where S_∞/S_0 is the CODEX signal at long mixing times, i.e., $t_m \gg t_c$, while f_m is the fraction of mobile species and W is the number of sites,[6,9] becomes invalidated.[21] Note that, in the absence of intermediate motions, for the LUV examined here, one predicts $f_m \rightarrow 1$ and $W \rightarrow \infty$ so that ideally $S_\infty/S_0 \rightarrow 0$.

Figure 8

Signal loss due to intermediate time scale motions during CODEX recoupling periods is related to "dynamic broadening" as observed under MAS. As discussed by Waugh and

coworkers for the case of isotropic rotational diffusion,[25] the intermediate motional regime, leading to maximum line broadening, is defined by the condition $\sqrt{2}\omega_r\tau_c \approx 1$.   In the present case, we observed that the line-width-at-half-height ($\Delta\nu_{1/2}$) of the isotropic resonance for LUV at 35°C was approximately a factor of three to four greater than found with corresponding MLV, as detailed in Table 1. This is consistent with the presence of intermediate time scale motions in the smaller LUV that are (largely) lacking in the larger MLV at this temperature. At 10°C, on the other hand, $\Delta\nu_{1/2}$ for the LUV and MLV were more equal, albeit greater than at 35 °C (see Table 1). Moreover, spinning LUV at a slower speed ($\nu_r = 2000\ Hz$) produced substantially broader lines (see Fig. S7), in accord with the predictions of Suwelak et al,[25] for the case of intermediate time scale motions.

A simple calculation further substantiates the notion that the presence of intermediate time scale motions, specifically lateral diffusion, produces the more rapid signal loss with increasing M in the case of LUV relative to MLV (and the differences in line width between MLV and LUV). Both overall vesicle tumbling and lateral diffusion around the vesicle's radius of curvature contribute to the rotational diffusion with rates as per Eq. (5). For a vesicle of radius 300 nm, at 35°C, assuming the viscosity of water, the correlation time for vesicle tumbling is on the order of 24 ms, i.e., somewhat long relative to the CODEX echo times used here to be considered an intermediate time scale motion. (Note that the effective viscosity within the packed confines of the MAS spinner is likely to be higher than that of pure water and, hence, the correlation time for overall vesicle tumbling is likely to be even longer than this estimate.) For the same size vesicle, assuming a typical lateral diffusion coefficient of $1\times10^{-11}\ m^2s^{-1}$, the correlation time for lateral diffusion is on the order of 1.5 ms. Thus, for a CODEX echo time of 616 μs, corresponding to $M=3$ and $\nu_r = 6500$ Hz, significant signal loss would be anticipated due to lateral diffusion. Given the distribution of LUV radii below 300 nm in Fig. 6, the ~50%

signal loss for the *M*=3 relative to the *M*=1 case evident in Fig. 8 becomes explicable. Additionally, as predicted by the simulations shown in Fig. 4A, for the vesicle sizes and lateral diffusion coefficients relevant here, lateral diffusion during the shortest possible mixing time, $t_m = t_r$, i.e. a single rotor period, causes significant intensity loss for the *M*=3 versus *M*=1 case.

The consequent bias towards larger radius vesicles in the recovered CODEX signal must be taken into account when extracting a lateral diffusion coefficient. To do so, we assume that the loss with increasing *M* is proportional to $\exp(-\tau_{echo}/\tau_c(R_i, D_{rot}))$, where $\tau_c(R_i, D_{rot})$ is given by Eq. (5), and then renormalize the lipid-radius population density accordingly.

4.3 Fitted CODEX ^{31}P NMR decays and phospholipid lateral diffusion coefficients.

The powder average approach, encompassing Eq.s (6) through (14), requires knowledge of the relevant CSA values. These were determined by simulating slow-spinning MAS spectra using the SIMPSON simulation program,[26] as detailed in Fig. S7. For liquid-crystalline DMPC in LUV at 35°C, i.e., in the liquid-crystalline phase, a value of $3/2\,\delta = 43.07$ ppm was determined, while at 10°C, i.e. in the gel phase, the corresponding value was 61.26 ppm. The increased CSA at 10°C is due to the larger order parameter in the gel phase, reflecting a decreased amplitude of off-axis "wobbling" of the lipid long axis. Note that rotation about the phospholipid long axis is still sufficiently fast at this temperature to produce an axially symmetric averaged chemical shift tensor, as evident in static ^{31}P NMR spectra (not shown). Note further that, while the CSA is readily obtained in the case of a "pure" phospholipid bilayer by simulating its static powder spectrum, in the case of "mixed" phospholipid bilayers, overlapping powder patterns render such an approach problematic. The slow-spinning MAS approach used here will be useful for evaluating the CSA of individual phospholipids in mixed

bilayers, provided they exhibit different isotropic chemical shifts, as indeed most phospholipid do.

Figure 9

In the experimental and simulation cases, the first point, at a mixing time of one rotor period, already exhibits signal attenuation (as predicted by simulations shown in Fig. 4A and demonstrated in the "master curves" in Fig. 8). In order to compare experiment and simulation, the experimental data were normalized such that the first experimental and simulation data points were equal. A weighted Chi-square analysis was employed to obtain the best fit lateral diffusion coefficient.

Fig. 9 shows experimental CODEX intensities measured with DMPC/AECHO, 95/5 (mol/mol) LUV obtained with M = 3, at temperatures both above (35 °C) and below (10 °C) the DMPC gel-to-liquid-crystalline phase transition. The powder average simulations provide satisfactory fits to the experimental data. The lateral diffusion coefficients extracted by this fitting are listed in Table 1 and indicate roughly a factor of 5 decrease in lateral diffusion in the gel phase relative to the liquid-crystalline phase of DMPC. This is in broad qualitative agreement with numerous literature results for DMPC lateral diffusion coefficients as reviewed by Tocanne et al.[27]

Quantitatively, in the liquid-crystalline state the lateral diffusion coefficients provided by CODEX are approximately 2-3 fold greater than consensus results from FRAP experiments.[27] On the other hand, they are approximately 4-5 fold smaller than values obtained via quasi elastic neutron scattering (QENS), as reviewed recently.[28] While various factors influence the lateral diffusion coefficient, including hydration, temperature, cholesterol, and proteins, the order of magnitude difference in FRAP versus QENS is attributed principally to time and length scale differences particular to each.[28] Specifically, FRAP (and related techniques) are "macroscopic"

in that they monitor lateral diffusion over time scales exceeding hundreds of milliseconds and length scales on the order of tens of microns. QENS, in contrast, is a "microscopic" method, in that it is sensitive to motions on the nanosecond time scale and length scales up to tens of nanometers. In the case of CODEX ^{31}P NMR, under the conditions employed here, the characteristic observation time scale is 1-10 rotor periods, equivalent to several milliseconds at most, corresponding to a length scale on the order of several hundred nanometers. Thus, the finding that the liquid-crystalline DMPC lateral diffusion coefficient measured by CODEX ^{31}P NMR lies intermediate to values obtained via FRAP and QENS, is consistent with the intermediate time and length scales of CODEX.

In the gel state, FRAP indicates that DMPC lateral diffusion slows by nearly 3 orders of magnitude.[27] QENS results indicate, however, that DMPC lateral diffusion slows by merely an order of magnitude upon entering the gel phase.[28] This contrast is attributed, again, to the different time and distance scales to which the two techniques are sensitive.[28] Our CODEX ^{31}P NMR results suggest an even more muted difference in DMPC lateral diffusion in the liquid-crystalline versus gel states then obtained via QENS. A portion of this may be due to the presence of 5 mol% AECHO in our LUV. From FRAP results, cholesterol is known to blunt differences in molecular dynamics between liquid-crystalline and gel states, slowing lateral diffusion in the liquid-crystalline state and enhancing it in the gel state.[29] However, the bulk of this effect occurs only at cholesterol concentrations exceeding 15-20 mol%. We postulate, therefore, that gel state DMPC lateral diffusion coefficient we measure reflect a combined effect of the presence of 5 mol% AECHO in our LUV and the time and length scale specifics of the CODEX ^{31}P NMR technique.

5 Conclusions

CODEX ^{31}P NMR measurements on DMPC/AECHO (95/5 mol/mol) LUV provide DMPC lateral diffusion coefficients, in both the liquid-crystalline and gel phases, consistent with established values, taking into account the particulars of time and length scale differences between techniques. Optimization of sample and NMR acquisition conditions has yielded profound sensitivity enhancements relative to our previous report,[7] and now permit rapid and routine lateral diffusion measurements of phospholipids in bilayer membranes. A powder average analysis of CODEX decay curves, based on the Gaussian-Diffusion-on-a-Sphere model,[8] as relevant to CODEX ^{31}P NMR measurements on a population of spherical unilamellar phospholipid bilayer vesicles displaying a distribution of vesicle radii, has been demonstrated to reliably simulate CODEX decay curves and yield lateral diffusion coefficients.

Further improvement in sensitivity would accrue from using even larger diameter vesicles, since the resulting lateral diffusion correlation times would then fall outside the intermediate time scale regime that produces detrimental signal loss during CODEX dephasing and rephasing time periods. While this would necessitate examining proportionately longer mixing times in order to obtain the desired lateral diffusion coefficient, the T_1 of the ^{31}P signal of the phospholipids, which is the ultimate limit on the mixing time, is longer still, by far.

A particular advantage of the CODEX ^{31}P NMR method is that in complex mixtures of different phospholipid species, such as found in nature, simultaneous measurements of individual lateral diffusion coefficients may be performed, provided the components exhibit different isotropic chemical shifts. To date, we have performed such measurements on mixtures of up to five different phospholipids, as will be reported shortly. This suggests the ability to examine

heterogeneities of phase, and/or specificity of protein/peptide interactions, in a single experiment, without the need for separate individual labeled species.

Beyond phospholipids, membrane protein or peptide lateral diffusion measurements via CODEX should be possible, in principle, but will require a judicious choice of isotopic labels (^{13}C, ^{15}N) placed such that the resulting chemical shift anisotropy is appropriate sized. For CODEX measurements of the effects of interactions between lipid bilayers and membrane proteins or peptides on lateral diffusion to succeed it will be necessary further to strike the correct balance between sample concentration, to achieve sufficient signal intensity, and sample dilution, to avoid

undue interlamellar interactions.

6 Acknowledgments

7 References

1   P.F.F. Almeida and W.L.C. Vaz, *Handbook of Biological Physics,* 1995, **1**, 305.

2   T.M. Jovin and W.L.C. Vaz, *Methods Enzym.*, 1989, **172**, 471.

3   N. Kahya and P. Schwille, *Molec. Memb. Biol.*, 2006, **23**, 29.

4   K. Ritchie, R. Iino, T. Fujiwara, K. Murase and A. Kusumi, *Molec. Memb. Biol.*, 2003, **20**, 13–18.

5   H.C. Gaede and K. Gawrisch, *Biophys. J.*, 2003, **85**, 1734.

6   E.R. deAzevedo, W.-G. Hu, T.J. Bonagamba and K.Schmidt-Rohr, *J. Amer. Chem. Soc.*, 1999, **121**, 8411.

7   Q. Saleem, A. Lai, H. Morales and P.M. Macdonald, *Chem. Phys. Lip.*, 2012, **165**, 721.

8   A. Ghosh, J. Samuel and S. Sinha, S. *Europhys. Lett.*, 2012, **98**, 30003-p1.

9   E.R. deAzevedo, W.-G. Hu, T.J. Bonagamba and K. Schmidt-Rohr, *J. Chem. Phys.*, 2000, **112**, 8988.

10   N. Bloembergen, E.M. Purcell and R.V. Pound, *Phys. Rev.*, 1948, **73**, 679.

11   A. Abragam. *Principles of Nuclear Magnetism,* Oxford, 1961.

12   M. Bloom, E.E. Burnell, M.I. Valic and G. Weeks, *Chem. Phys. Lip.*, 1975, **14**, 107.

13   M. Munowitz and R.G. Griffin, *J. Chem. Phys.*, 1982, **76**, 2848.

14   M.E. Rose, *Elementary Theory of Angular Momentum*, 1957, Wiley, New York.

15   C. Dolainsky, P. Karakatsanis and T.M. Bayerl, *Phys. Rev. E*, 1997, **55**, 4512.

16   Q. Saleem, Z. Zhang, C.C. Gradinaru and P.M. Macdonald, P. M. *Langmuir* 2013, **29**, 14603.

17   J.F. Popplewell, M.J. Swann, N.J. Freeman, C. McDonnell and R.C. Ford, *Biochim. Biophys. Acta - Biomembr.*, 2007, **1768**, 13.

18   K.R. Thurber and R. Tycko, *J. Magn. Reson.*, 2009, **196**, 84.

19   A.E. Bennett, C.M. Rienstra, M. Auger, K.V. Lakshmi and R.G. Griffin, *J. Chem. Phys.*, 1995, **103**, 6951

20   M. Wachowicz, L. Gill and J.L.White, *Macromolecules,* 2009, **42**, 553.

21   K. Saalwächter and I. Fischbach, *J. Magn. Reson.*, 2002, **157**, 17.

22   C. Hackel, C. Franz, A. Achilles, K. Saalwächter and D. Reichert, *Phys. Chem. Chem. Phys.*, 2009, **11**, 7022.

23   C.P. Jaroniec, B.A. Tounge, C.M. Rienstra, J. Herzfeld and R.G. Griffin, *J. Magn. Reson.*, 2000, **146**, 132.

24   A.G. Marshall and F.R. Verdun, *Fourier Transforms in NMR, Optical, and Mass*

Spectrometry, Elsevier, Amsterdam, 1990.

25   D. Suwelack, W. P. Rothwell and J. S. Waugh, *J. Chem. Phys.*, 1980, **73**, 2559.

26   M. Bak, J.T. Rasmussen and N.C. Nielson, *J. Magn. Reson.* 2000, **147**, 296.

27   J.-F. Tocanne, L. Dupou-Cézanne and A. Lopez, *Prog. Lipid Res.* 1994, **33**, 203.

28   V.K. Sharma, E. Mamontov, D.B. Anunciado, H. O'Neill and V. Urban, *J. Phys. Chem. B,* 2015, **119**, 4460.

29   J.L.R. Rubenstein, B.A. Smith and H.M. McConnell, *Proc. Natl. Acad. Sci. USA*, 1979, **76**, 15.

Table 1

Comparison of certain ^{31}P NMR spectral properties from DMPC/AECHO (95/5, mol/mol) in the form of MLV versus LUV.

Property	MLV		LUV	
Temperature °C	10	35	10	35
$\Delta\nu_{1/2}$ (Hz)	158	19	117	76
T_2^* (ms)	2.0	19.9	2.7	4.2
T_2^{rc} (ms)	0.96	1.31	0.61	0.43
D$_{lat}$ (m^{2}s^{-1})	-	-	2.8×10^{-12}	1.3×10^{-11}

8 Figure Captions

Figure 1.   The CODEX ^{31}P NMR pulse sequence, adapted from deAzevedo et al.[6] Direct

excitation, rather than cross polarization, was employed with the phase cycle adjusted

accordingly.[20] TPPM proton decoupling[19] was applied during the recoupling and acquisition

periods. All pulses were strictly synchronized with the rotor period, t_r. The number of 180°

pulses applied during a given recoupling period was $M = 1, 3, 5...$, where $M = 2m+1$; each 180°

pulse being separated by one half rotor period $(t_r/2)$. The mixing time $t_m = Nt_r$ was a multiple

of the rotor period. A z-filter of duration $t_z = t_r$ was inserted prior to acquisition.

Figure 2.   Orientation of the unique axis of the chemical shift tensor $\boldsymbol{\sigma_z}$ in the rotor frame of

reference (after Munowitz and Griffin[13]), before and after a diffusive jump.   The polar and

azimuthal angles, β_i and α_i, respectively, define the initial and final orientations, $i = 1,2$

respectively, of $\boldsymbol{\sigma_z}$ relative to the rotor frame.   The rotation axis is oriented at the magic angle

relative to the magnetic field $\mathbf{B_o}$. The diffusive jump is defined relative to the reference frame of

the initial orientation by the polar and azimuthal angles, θ and φ, respectively.

Figure 3.   Probability density of the diffusive jump angle θ for various mixing times

$t_m = Nt_r$ as calculated using the "Gaussian-Diffusion-on-a-Sphere" equations of Ghosh et al.[8]

Calculations were performed for a vesicle radius $R = 350$ nm, a lateral diffusion coefficient $D_{lat} =$

1.0×10^{-12} m^{2}s^{-1}, a rotor period $t_r = 154$ μs ($v_r = 6500$ Hz) and values of $N = 1$ (black), 3 (red), 10

(green) and 25 (blue).

Figure 4.   (A)   Calculated CODEX signal intensity for individual pairs of angles β_1 and θ,

corresponding, respectively, to the initial position of the unique chemical shift tensor component

σ_z and the diffusive jump angle. Values of $cos(|\Phi_2| - |\Phi_1|)$ were calculated as described in the text for the specific case $M = 3, \frac{3}{2}\delta = 45\ ppm$ and $v_r = 6500\ Hz$.

(B)   Normalized joint probability $P(\beta)P(\theta)$ for individual pairs of angles β_1 and θ. $P(\beta) = sin\beta$ is the geometric probability distribution on a sphere. $P(\theta)$ is the diffusive jump angle probability calculated using the "Gaussian-Diffusion-on-a-Sphere" equations of Ghosh et al,[8] here for the specific case of a vesicle radius $R = 350$ nm, a lateral diffusion coefficient $D_{lat} = 1.0\text{x}10^{-11}\ m^2s^{-1}$, a rotor period $t_r = 154$ μs ($v_r = 6500$ Hz) and a mixing time $t_m = 3t_r$.

(C)   Probability-weighted CODEX signal intensity for individual pairs of angles β_1 and θ. The powder-averaged CODEX signal intensity, given the parameter values in (A) and (B) above, is simply the sum of $P(\beta)P(\theta)(cos(|\Phi_2| - |\Phi_1|))$ over all values of β_1 and θ.

Figure 5.   Simulations of powder-average CODEX signal decays with increasing mixing time using the Gaussian-Diffusion-on-a-Sphere model,[8] as a function of the principle experimental and sample variables.

(A)   Various number of recoupling pulses M (circles $M = 1$, squares $M = 3$, triangles $M = 5$): otherwise, $\frac{3}{2}\delta = 45\ ppm$, $R = 350$ nm, $D_{lat} = 1\text{x}10^{-11}m^2s^{-1}$.

(B)   Various chemical shift anisotropies (circles $\frac{3}{2}\delta = 30\ ppm$, squares $\frac{3}{2}\delta = 45\ ppm$, triangles $\frac{3}{2}\delta = 60\ ppm$): otherwise, $M = 3$, $R = 350$ nm, $D_{lat} = 1\text{x}10^{-11}m^2s^{-1}$.Various vesicle radii R (circles 700 nm, squares 350 nm, triangles 175 nm): otherwise $M = 3$, $\frac{3}{2}\delta = 45\ ppm$, $D_{lat} = 1\text{x}10^{-11}m^2s^{-1}$.

(C)   Various lateral diffusion coefficients D_{lat} (circles $1\text{x}10^{-13}m^2s^{-1}$, squares $1\text{x}10^{-12}m^2s^{-1}$, triangles $1\text{x}10^{-11}m^2s^{-1}$, diamonds $5\text{x}10^{-11}m^2s^{-1}$): otherwise $M = 3$, $\frac{3}{2}\delta = 45\ ppm$, $R = 350$ nm.

Figure 6.   DLS determined number average vesicle radius probability distribution (cyan bars) and corresponding lipid population probability distribution (pink bars). The normalized number average vesicle radius probability, $P(R_i)$, obtained from DLS, was converted to lipid average radius probability, i.e., the probability that a lipid will be resident in a vesicle of a given radius, by scaling with respect to the vesicle surface area (both inner and outer leaflets), $8\pi R_i^2$, and renormalizing.

Figure 7.   CODEX ^{31}P NMR spectra ($M = 3$) for LUV composed of DMPC/AECHO, 95/5, mol/mol, at 35°C. The lower row shows the effects of increasing mixing time $t_m = Nt_r$, where $t_r = 154\ \mu s$ is the MAS rotor period at $\nu_r = 6500\ Hz$, for a constant value of the z-filter, $t_z = t_r$. The upper row shows the corresponding reference spectra in which the mixing time was held constant at $t_m = t_r$, while the duration of the z-filter was increased as $t_z = Nt_r$. The corresponding spectral series for LUV at 10°C is provided in Fig. S2.

Figure 8.   CODEX ^{31}P NMR "master curves," showing signal intensity as a function of the duration of the recoupling period: $\tau_{echo} = t_r(M + 1)$, $M = 1, 3, 5....$, with $t_r = 154$ μs and $t_m = t_z = t_r$, for MLV (circles) and LUV (squares) at 10°C (open symbols) and at 35°C (closed symbols). Lines of fit correspond to $\exp(-\tau_{echo}/T_2^{rc})$, where T_2^{rc} is an apparent recoupling relaxation time, values of which are listed in Table 1.

Figure 9.   CODEX ^{31}P NMR signal intensity from DMPC/AECHO, 95/5, mol/mol LUV at 10 °C (circles) and at 35 °C (squares), for M=3, as a function of the duration of the mixing time: $t_m = Nt_r$ with $t_r = 154$ μs. Lines of fit were generated using the powder average simulation as

described in the text with a lateral diffusion coefficient D_{lat} = 2.8x10^{-12}m^{2}s^{-1} at 10°C and 1.3x10^{-11}m^{2}s^{-1} at 35°C.
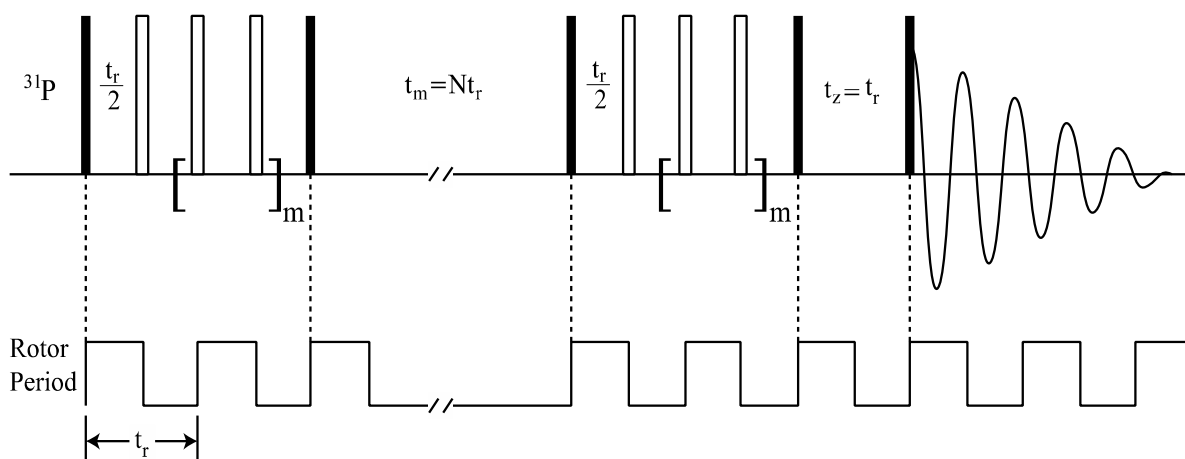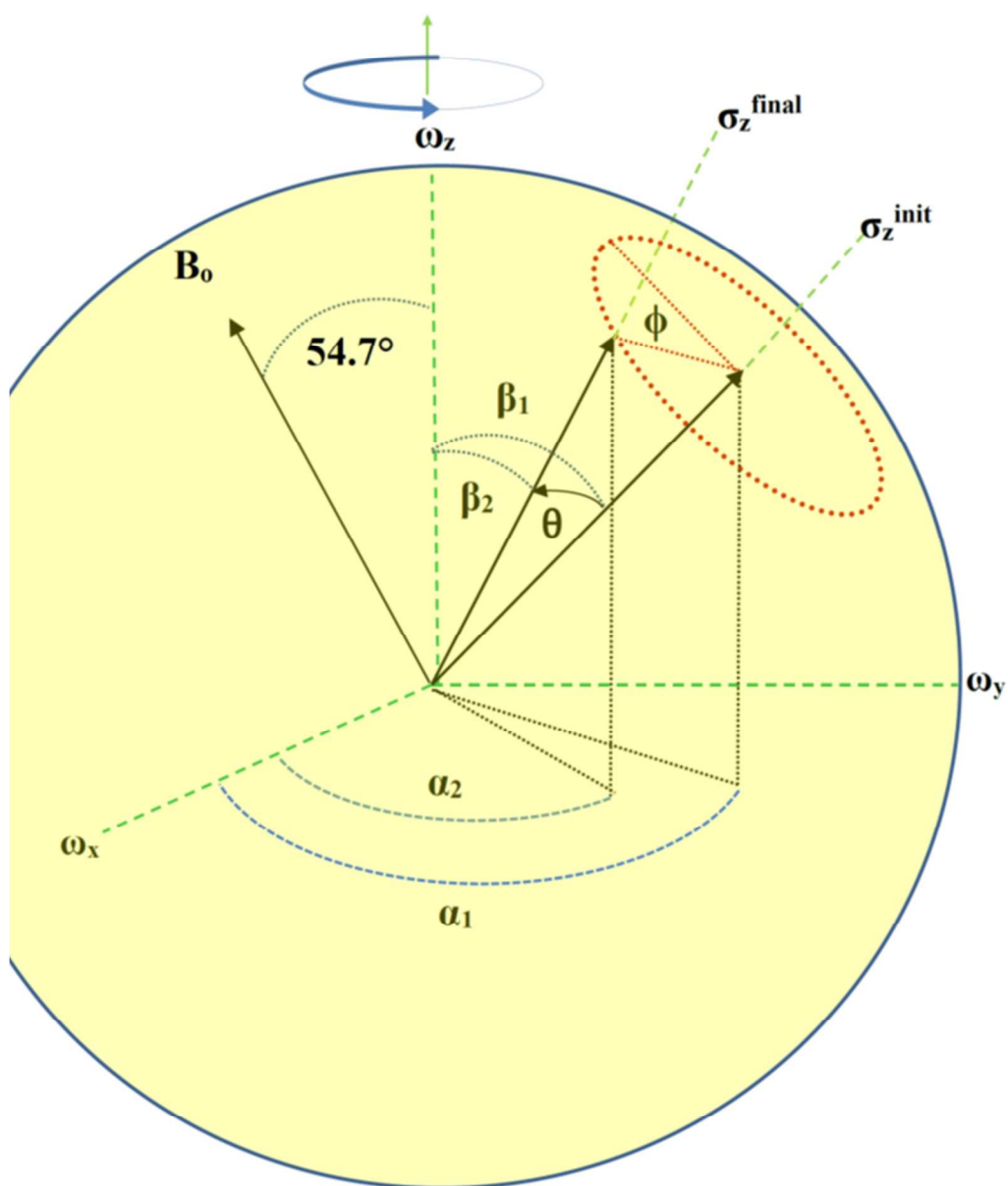

Figure 1 Lai et al
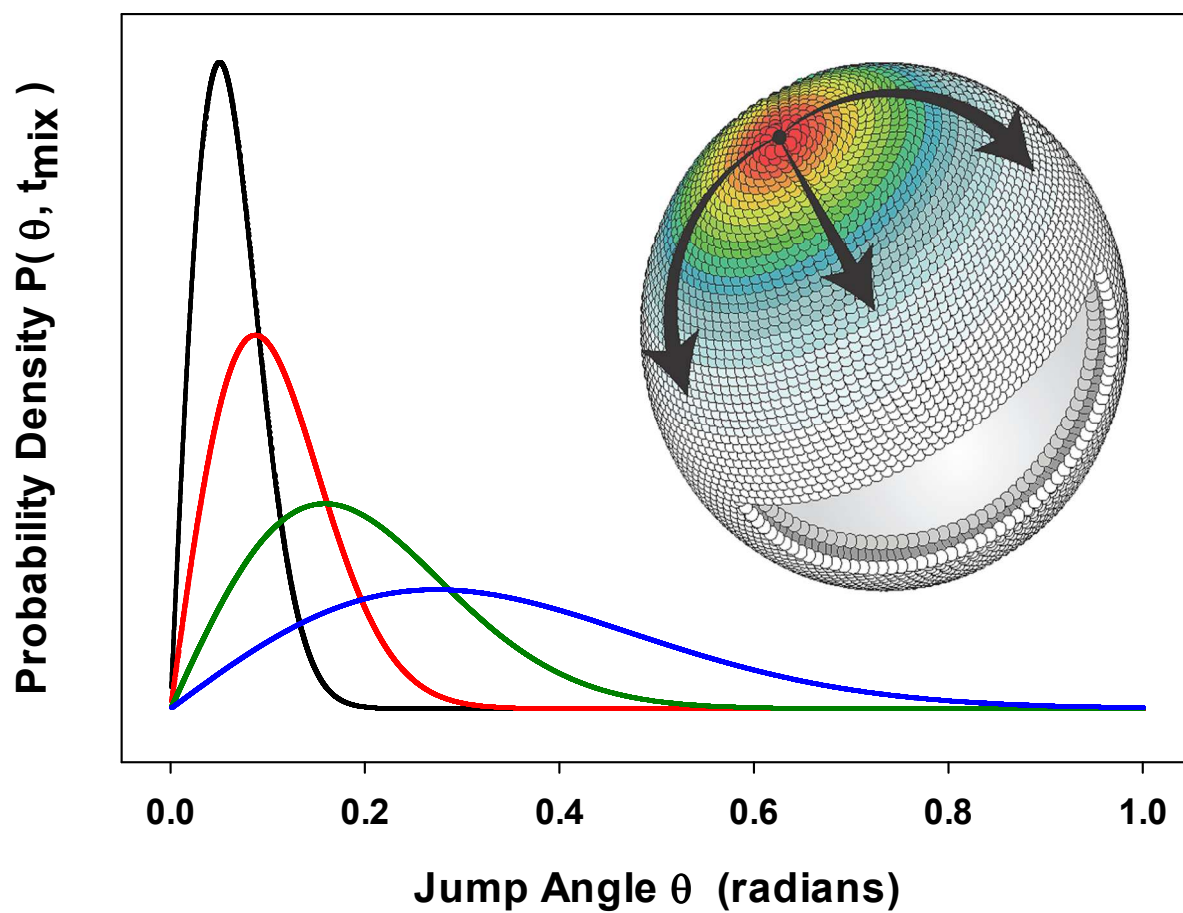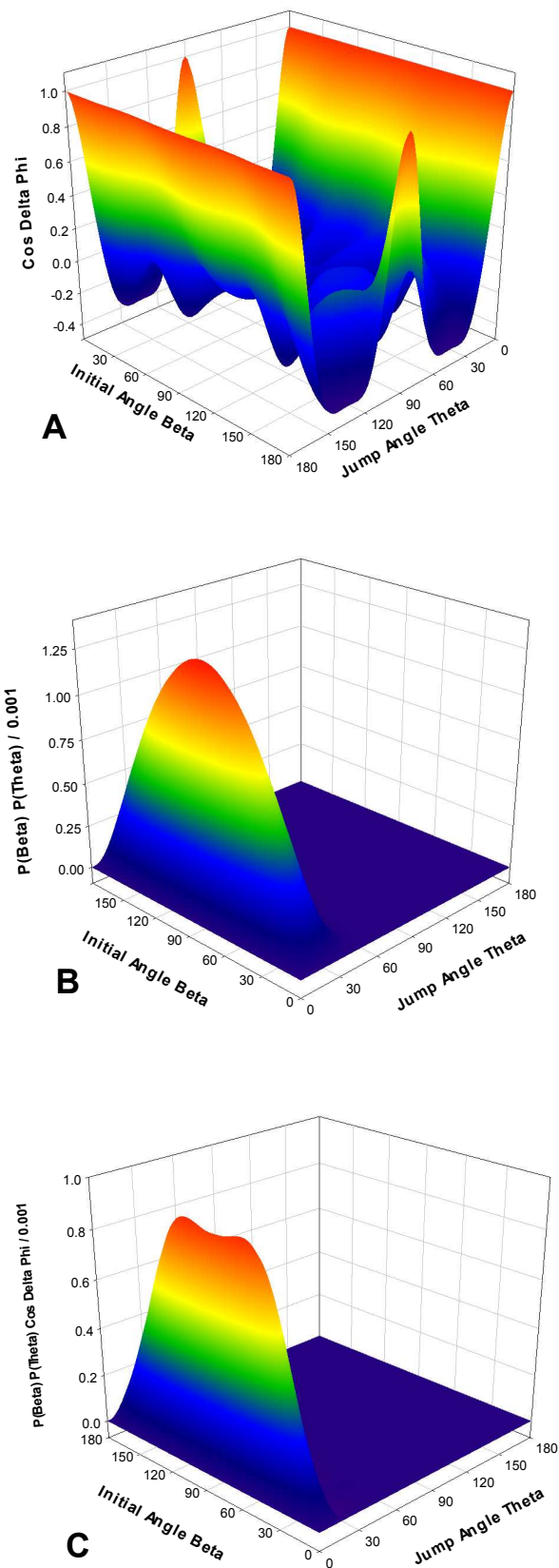
34

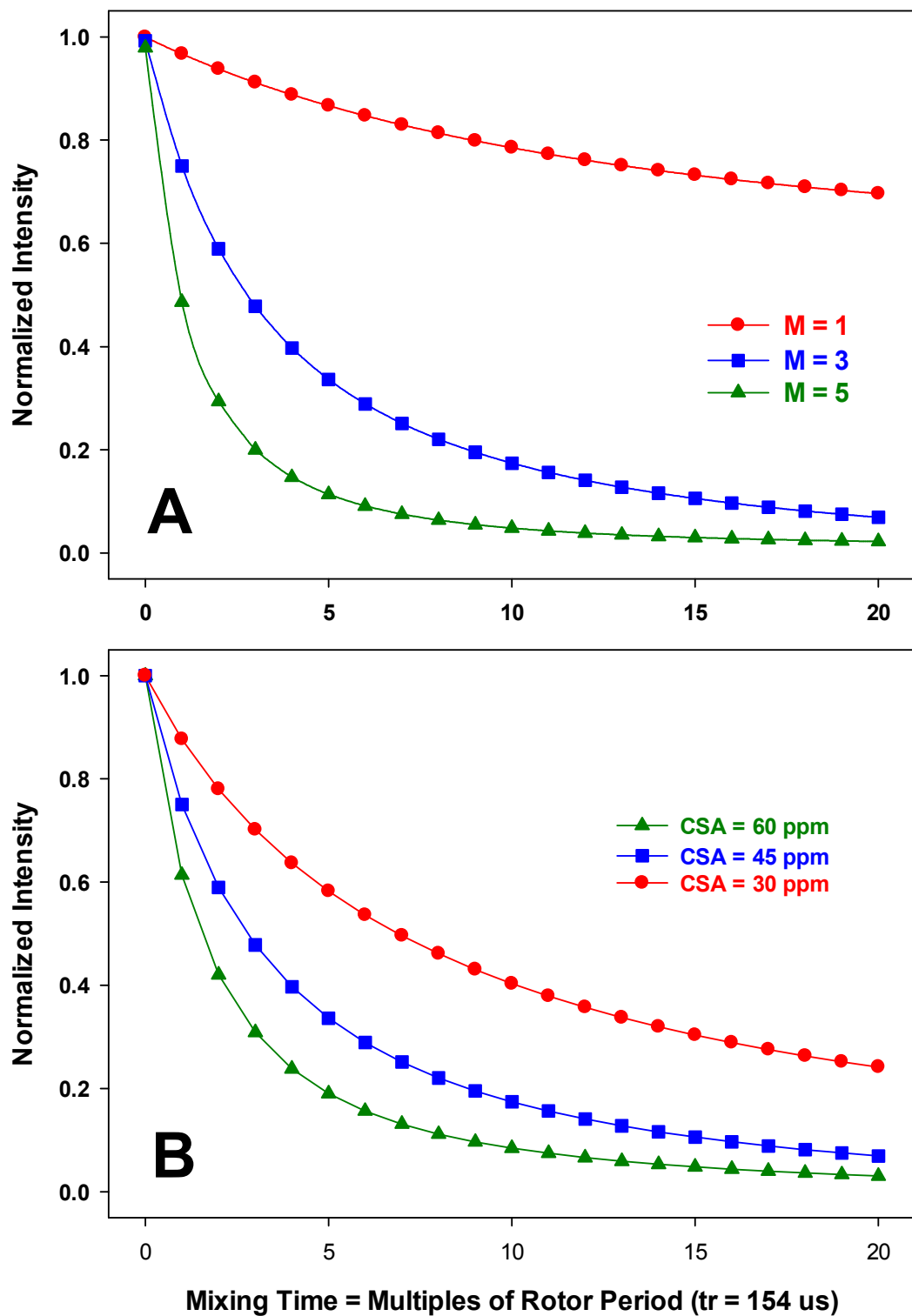Figure 2 Lai et al.

Figure 3 Lai et al.

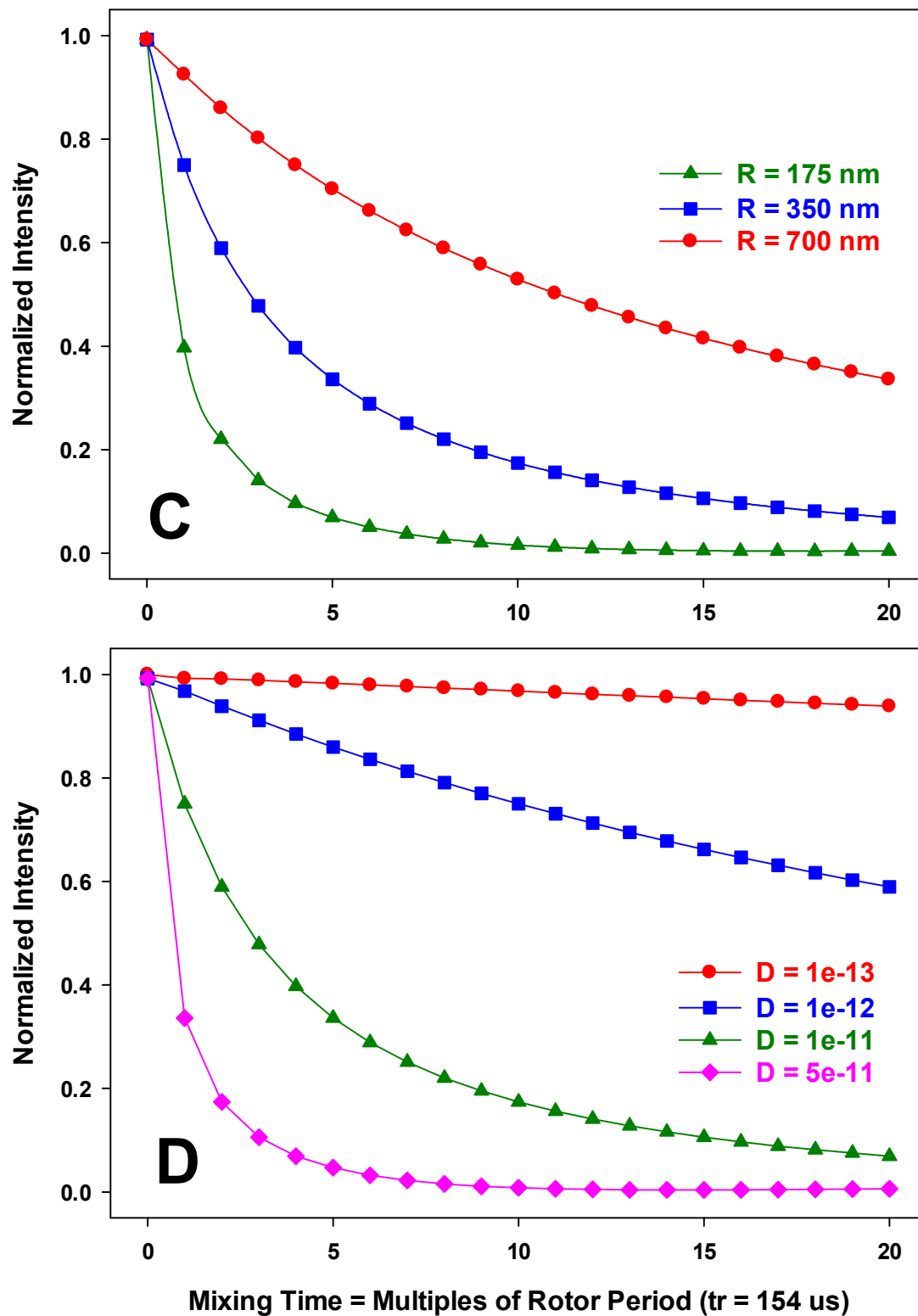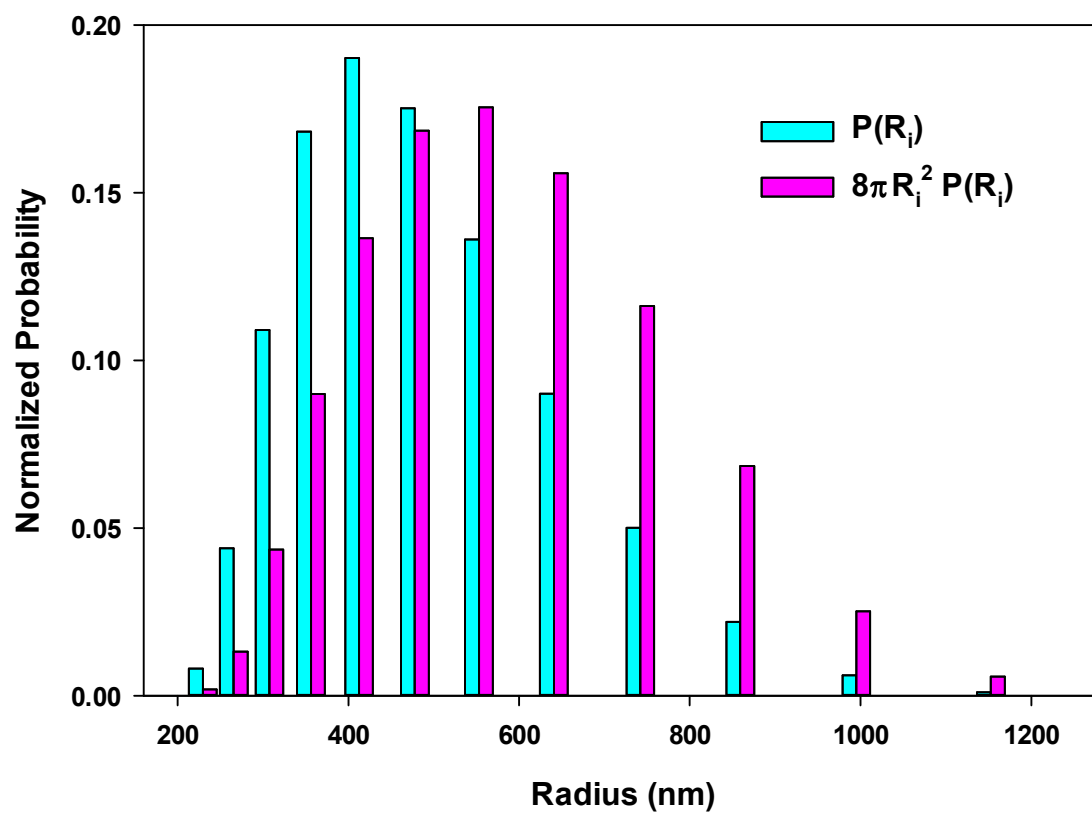Figure 4 Lai et al

Figure 5 Lai et al.
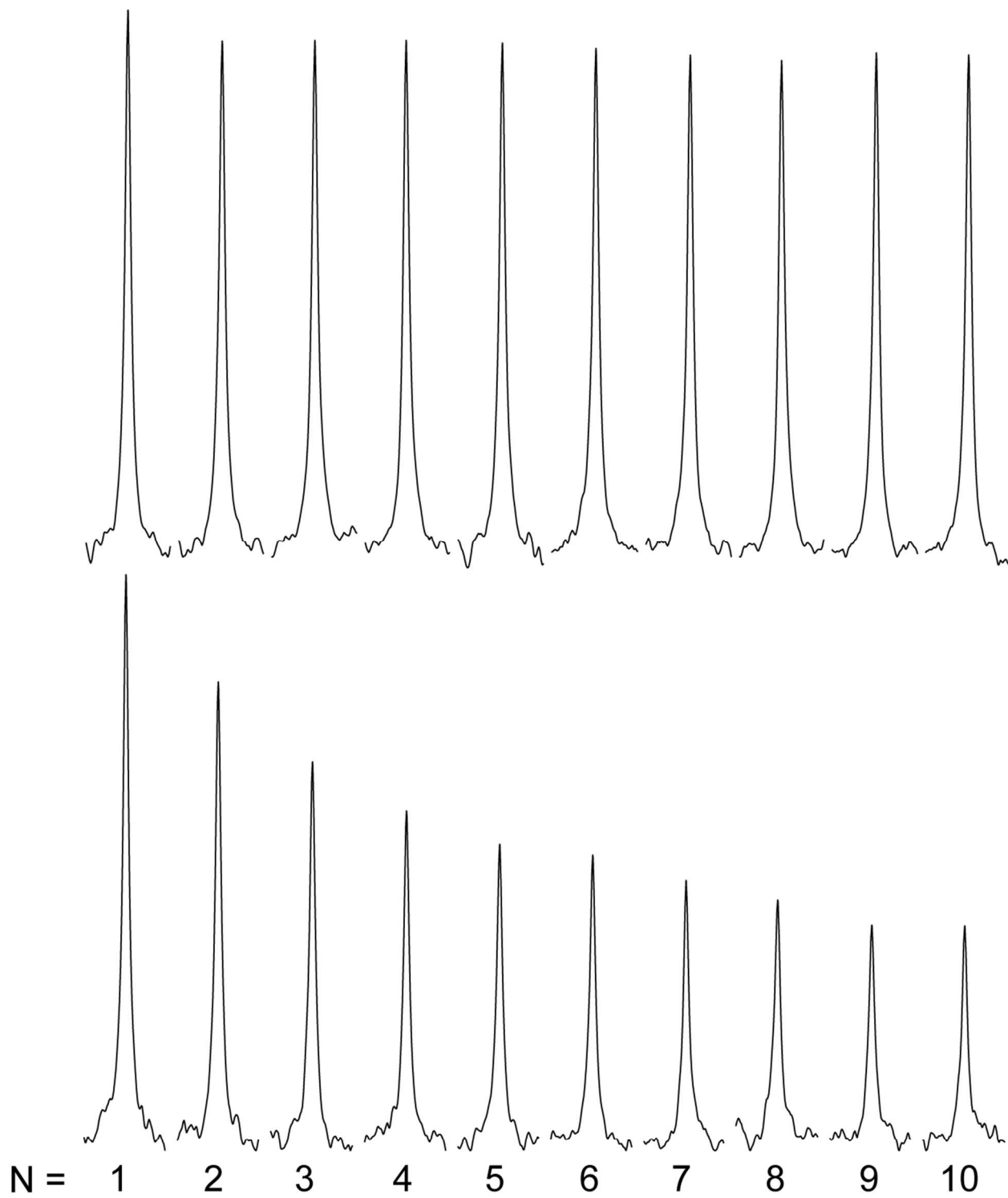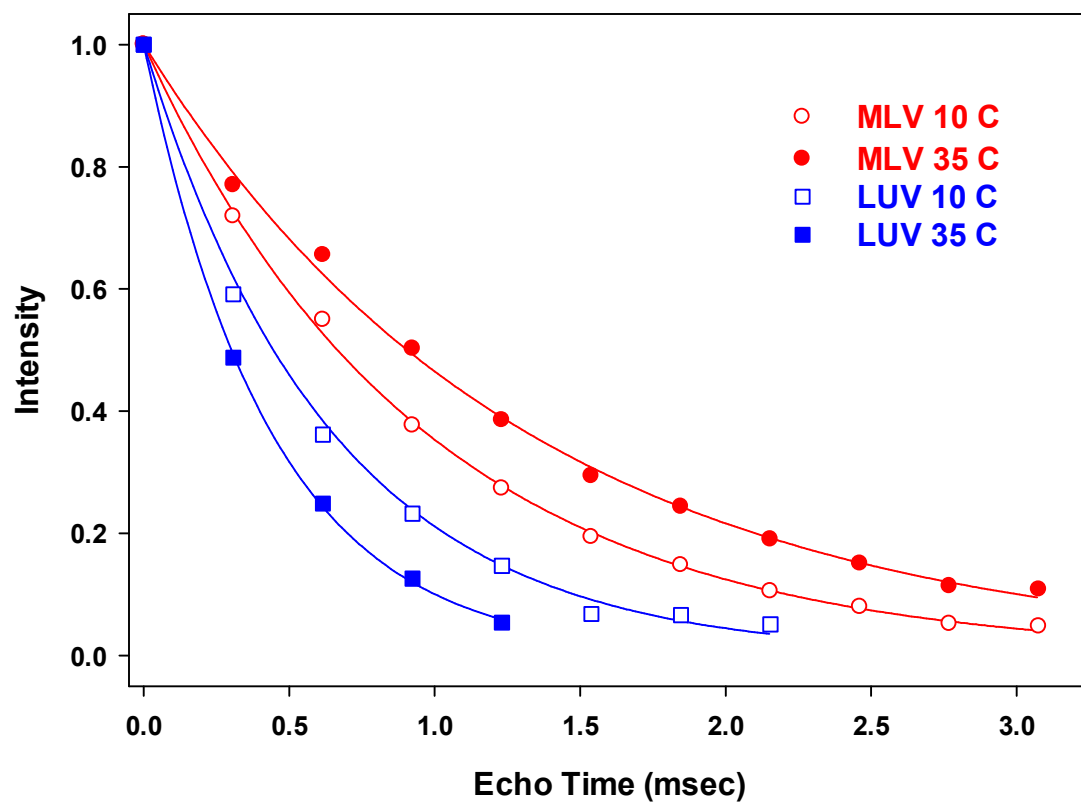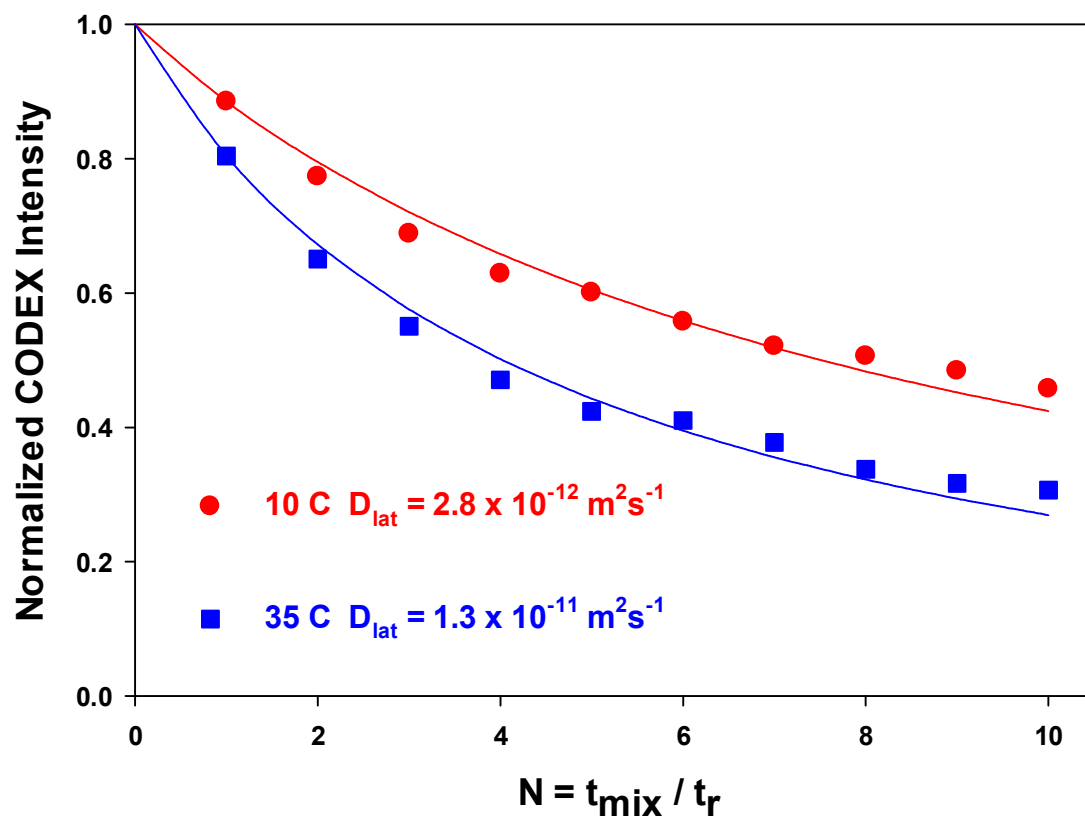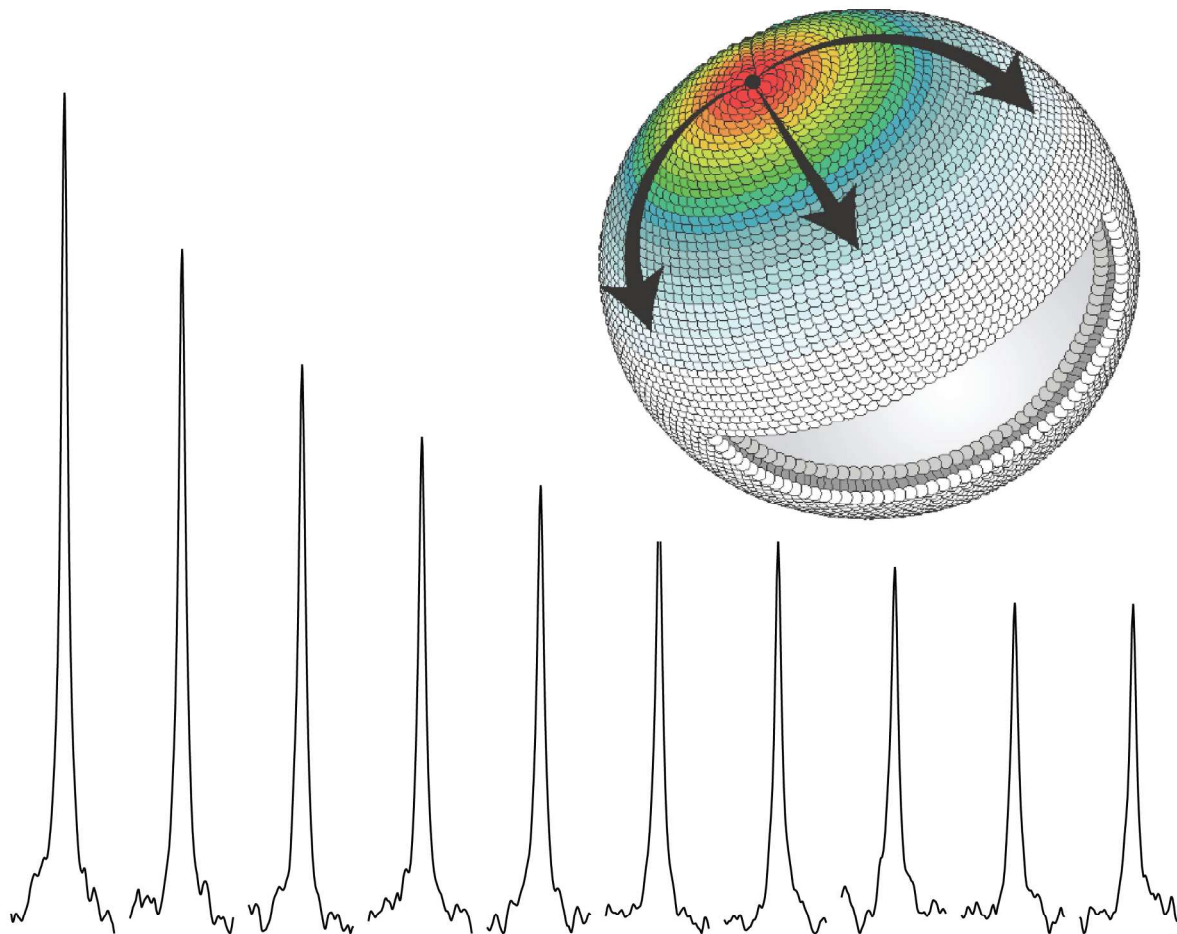
Figure 5 cont'd Lai et al.

Figure 6, Lai et al.

Figure 7 Lai et al

Figure 8   Lai et al.

Figure 9 Lai et al.

TOC Graphic